

Article

The Effects of Annealing Temperature on the Structural Properties of ZrB₂ Films Deposited via Pulsed DC Magnetron Sputtering

Wei-Chun Chen *, Chao-Te Lee, James Su and Hung-Pin Chen

Taiwan Instrument Research Institute, National Applied Research Laboratories, 20. R&D Rd. VI, Hsinchu Science Park, Hsinchu 30076, Taiwan; tigerlee@narlabs.org.tw (C.-T.L.); sujames@narlabs.org.tw (J.S.); chbin@tiri.narl.org.tw (H.-P.C.)

* Correspondence: weichun@narlabs.org.tw; Tel.: +886-3-5779911 (ext. 646)

Received: 26 March 2019; Accepted: 15 April 2019; Published: 16 April 2019



Abstract: Zirconium diboride (ZrB₂) thin films were deposited on a Si(100) substrate using pulsed direct current (dc) magnetron sputtering and then annealed in high vacuum. In addition, we discussed the effects of the vacuum annealing temperature in the range of 750 to 870 °C with flowing N₂ on the physical properties of ZrB₂ films. The structural properties of ZrB₂ films were investigated with X-ray diffraction (XRD), field emission scanning electron microscopy (FE-SEM), transmission electron microscopy (TEM), atomic force microscopy (AFM), and X-ray photoelectron spectroscopy (XPS). The XRD patterns indicated that the ZrB₂ films annealed at various temperatures exhibited a highly preferred orientation along the [0001] direction and that the residual stress could be relaxed by increasing the annealing temperature at 870 °C in a vacuum. The surface morphology was smooth, and the surface roughness slightly decreased with increasing annealing temperature. Cross-sectional TEM images of the ZrB₂/Si(100) film annealed at 870 °C reveals the films were highly oriented in the direction of the c-axis of the Si substrate and the film structure was nearly stoichiometric in composition. The XPS results show the film surfaces slightly contain oxygen, which corresponds to the binding energy of Zr–O. Therefore, the obtained ZrB₂ film seems to be quite suitable as a buffer layer for III-nitride growth.

Keywords: ZrB₂; DC sputtering; annealing

1. Introduction

Zirconium diboride (ZrB₂) is a relatively stable compound possessing a hexagonal crystal structure (AlB₂ structure, P6/mmm), and its *a*-axis lattice parameter ($a = 3.169 \text{ \AA}$) is very close to that of GaN ($a = 3.189 \text{ \AA}$) [1]. It has recently attracted widespread interest because its in-plane lattice parameter and thermal-expansion coefficient reasonably match those of GaN [2]. Specifically, its in-plane lattice parameter has only a 0.6% mismatch with that of GaN. In addition, the thermal expansion coefficients of ZrB₂ and GaN along on the basal plane are also well matched, namely, 5.9×10^{-6} and $5.6 \times 10^{-6} \text{ K}^{-1}$, respectively. Thus, using a ZrB₂(0001) buffer layer represents an important strategy for growing high-quality GaN on Si. Moreover, GaN films with low defect densities have reportedly been grown on ZrB₂ [3]. In addition, the epitaxial growth of a ZrB₂ buffer layer on Si(111) enables the technologically relevant monolithic integration of GaN with Si, which is economical and widely employed.

In addition, ZrB₂ is a very stable compound with high hardness and a high melting temperature (3220 °C), which is desirable for growing III-nitrides at a high growth temperature. If a single-crystalline ZrB₂ layer could be grown on a Si substrate, this layer could serve as a lattice-matched buffer layer as well as a thermally stable electrode for GaN-related devices, similar to Al_{0.25}Ga_{0.75}N [4]. On the other

hand, the very low resistivity of ZrB₂, even in the form of a thin film [5], allows good charge carrier injection and efficiently dissipates heat. In addition, the highly reflective nature of the ZrB₂ buffer layer ensures no light is lost through the Si substrate, and its metallic nature enables its use as an ohmic contact in nitride devices such as light-emitting diodes (LEDs) by providing a vertical current path and simplifying the LED geometry. Recently, a vertical device setup using thermally and electrically conductive substrates were proposed to overcome the low saturation of the device [6,7].

Previous studies on the growth of ZrB₂ films showed that ZrB₂ can grow epitaxially on a Si(111) substrate with MBE [8]. Moreover, Bera et al. reported that conductive, single-crystalline ZrB₂ thin films can be grown on insulating sapphire with thermally decomposing Zr(BH₄)₄ using the ultrahigh vacuum chemical vapor deposition (UHV-CVD) method [9]. However, due to its high melting point and violent evaporation at the melting point, the growth of single-crystal ZrB₂ is very difficult. Otani et al. studied the bulk growth of various metal borides using a floating-zone (FZ) method [10]. Meanwhile, Stewart et al. reported that in e-beam co-evaporation, the evaporated flux should be ~60% Zr to achieve films near-stoichiometric ZrB₂ [11]. Recently, Tengdelius et al. grew stoichiometric ZrB₂ using direct current (dc) magnetron sputtering [12]. However, they found that attaining a clean, well-ordered surface was challenging, especially with respect to oxygen contamination. However, Sulyaeva et al. indicated the oxide layer formed by exposing the film to air can be removed by annealing under UHV [13]. Armitage et al. demonstrated a cleaning process for the ZrB₂(0001) surface utilizing an HF solution treatment combined with lower-temperature (1000 °C) annealing [14]. Nevertheless, these methods are impractical for cleaning ZrB₂ substrates to be used for GaN epitaxy because they require special equipment that is not available for GaN growth reactors.

In this study, we investigate the influence of the annealing temperature on ZrB₂ thin films deposited on a Si substrate under high vacuum. The effectiveness of this method is evaluated using X-ray diffraction (XRD), field emission scanning electron microscopy (FE-SEM), atomic force microscopy (AFM), transmission electron microscopy (TEM), and X-ray photoelectron spectroscopy (XPS).

2. Materials and Methods

Hexagonal ZrB₂ thin films were deposited on mirror-like Si(100) substrates using pulsed dc magnetron sputtering at 500 °C without a bias voltage. Mirror-like Si(100) with dimensions of 20 mm × 20 mm was chosen as the substrate. The sputtering vacuum chamber was equipped with a turbo-pump to reduce the pressure to ~6.7 × 10⁻⁵ Pa. A ZrB₂ compound target (99.95% purity) was reactively sputtered in high-purity Ar (99.999%) gas at 10 sccm. Therefore, the growth temperature was set at 500 °C to grow ZrB₂ films for 30 min at a working pressure of 6.7 × 10⁻¹ Pa. The distance between the substrate holder and the target was 7 cm. The target diameter was 7.62 cm. The magnetron field for the sputtering source was about 1000–1500 G. The dc power, frequency and reverse time were fixed at 150 W, 70 kHz and 2 μs, respectively. For the pulsed DC power supply, the frequency is similar to RF sputtering. The frequency ranges from 10 to 200 kHz are typically used for pulsed DC power supply and 13.5 MHz is the main frequency for RF sputtering. The Ar gas flow was independently controlled using mass-flow controllers. Before deposition, the Si(100) substrates were ultrasonically cleaned in acetone and ethanol and dried with dry N₂. Then, the substrate was wet-etched in a buffered oxide etch (BOE) for 1 min before being placed into the vacuum chamber. Prior to ZrB₂ growth, the Si(100) substrate was heat-treated in the chamber under a vacuum of 6.67 × 10⁻⁵ Pa at 700 °C for 1 h, and the target was sputtered to clean the surface for 10 min with a shutter covering the substrate. For the deposition, all ZrB₂ films were deposited on Si(100) at 500 °C for 30 min using a resistance heater. The as-grown ZrB₂ film was divided into four samples with the same area. Next, each ZrB₂ film was inserted into a high-vacuum chamber (1.33 × 10⁻⁷ Pa) and annealed in 1 sccm of N₂ flow ratio (corresponding to 1.33 × 10⁻³ Pa). Three of the ZrB₂ samples were separately annealed for 1 h at 750, 810, and 870 °C, respectively. Then, the sample was cooled down to room temperature under vacuum. For all annealing experiments, the temperature ramp-up rate was 30 °C/min, and the cool-down rate was 50 °C/min. In addition, the substrate temperature was monitored using a calibrated infrared

pyrometer with the sample surface. Additionally, a thermocouple is used to measure the backing plate of the heater in close contact. In this study, all annealing temperatures were displayed in an infrared pyrometer with a PID-programmable heater.

In the article, we report the high vacuum annealing temperature of ZrB₂ films on Si(100) using DC magnetron sputtering. The structural properties of the ZrB₂ films were examined using XRD (Bruker D8, Hamburg, Germany) in the θ - 2θ mode with Cu K α radiation in the range 20–80° of 2θ . The lattice parameters of ZrB₂ films were calculated from the high-resolution XRD mode. The diffraction angle 2θ was scanned from 20° to 30° at 0.02°/s. The cross-sectional surface morphology and microstructure of the deposited ZrB₂ films were analyzed via FE-SEM (Hitachi S-4300 FE-SEM, Hitachi, Ltd., Chiyoda-ku, Japan) and FE-TEM (Philips Tecnai 20, Philips, Amsterdam, The Netherlands). The focused ion beam technique was used to prepare the cross-sectional TEM specimens. Atomic force microscopy (AFM) in the tapping mode was used to investigate the surface morphology and roughness of the films. The XPS experiments were performed in a VG ESCA Scientific Theta Probe using Al K α ($h\nu = 1486.6$ eV) radiation to characterize the bonding characteristics of elements in the films.

3. Results and Discussion

Figure 1a shows the XRD $\theta/2\theta$ diffractograms of the all ZrB₂/Si(100) films, both as-grown and annealed at various temperatures. The pattern shows three peaks at $2\theta = 25.16 \pm 0.05^\circ$, $2\theta = 51.68 \pm 0.05^\circ$ and $2\theta = 69.26 \pm 0.05^\circ$ corresponding to ZrB₂(0001), ZrB₂(0002), and the Si(004) substrate in all ZrB₂ films, respectively, suggesting that they are preferentially oriented in the *c*-axis direction. Thus, the XRD results indicate that the films possess a high *c*-axis-orientated hexagonal crystal structure. These results are similar to those of Samuelsson et al., who reported ZrB₂ films deposited on a Si(100) substrate [15].

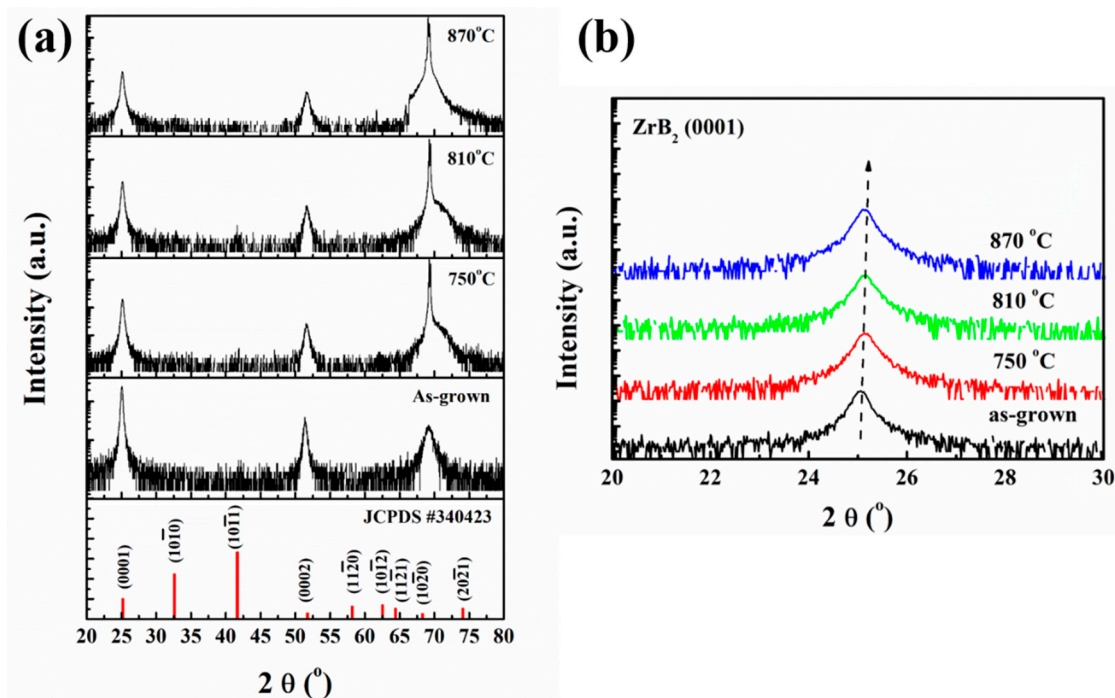


Figure 1. All ZrB₂ films deposited on Si(100) as-grown and annealed at various temperatures. (a) θ - 2θ X-ray diffraction (XRD) pattern of all ZrB₂ films and JCPDS#340423; (b) XRD pattern for the (0001) peak of all ZrB₂ films in the 2θ range of $\sim 22^\circ$ to 30° .

Figure 1b exhibits shifts in the (0001) peak towards higher diffraction angles, which suggest that the films are in a state of tensile residual stress [16]. This observed residual stress is due to energetic bombardment using Ar ions during sputtering. In addition, the *c*-axis lattice parameters of ZrB₂ films were calculated from the (0001) lattice plane. The XRD pattern of the as-grown ZrB₂ film exhibits

slightly shifted broad peaks, which indicate a large *c*-axis lattice parameter. Moreover, the broad peaks reveal the poor crystallinity and residual stress of the film.

On the other hand, when the annealing temperature increased from 750 to 870 °C, the *c*-axis lattice parameter of ZrB₂ films slightly decreased from 3.556 to 3.545 Å. The latter value is close to the *c*-axis lattice constant of bulk ZrB₂, which was reported to be 3.530 Å, [17] suggesting that the strain of ZrB₂ was almost relaxed after the annealing.

In addition, XRD profiles are used to measure the average crystallite size of the sample. For all the ZrB₂ films annealed at various temperatures, the crystallite size was calculated from XRD profiles from reflections with a strong intensity percentage by measuring the full width at half maximum (FWHM) of the relevant peaks. The Debye–Scherrer equation for calculating the crystallite size is given by Equation (1) [18],

$$d = \frac{0.9\lambda}{B \cos \theta_B} \quad (1)$$

where λ is the X-ray wavelength of 1.54 Å, θ_B is the Bragg diffraction angle, and B is the FWHM of the peak at θ_B . The calculated average crystallite sizes of the as-grown samples and those annealed at 750, 810, and 870 °C are 24.8, 25.3, 25.5 and 28.3 nm, respectively. Thus, the crystallite size of ZrB₂ slightly increased with the increasing annealing temperature, which can be understood as due to the merging process induced by thermal annealing. ZrB₂ films contain many dangling bonds related to the zirconium and boron defects at the grain boundaries. These defects are favorable to the merging process to form larger ZrB₂ grains with the increasing annealing temperature.

Figure 2 shows the SEM micrographs of the surface morphologies and AFM images of the surface roughness of all the ZrB₂ films. The surface morphology (including surface roughness, waviness and surface non-uniformities) of ZrB₂ films was clearly smooth. Additionally, all the ZrB₂ films exhibit fairly smooth surface morphologies, regardless of the annealing temperature. On the other hand, the cross-sectional images indicated that the as-grown ZrB₂ and annealed at 870 °C of ZrB₂ films were about 420 ± 10 nm thick. The ZrB₂ film still appears to be continuous without any delamination from the substrate and its thickness of 420 nm remains almost unchanged, implying that ZrB₂ is thermally and physically stable at high annealing temperatures. In addition, the ZrB₂ surfaces appear to be free of cracks after all the annealing treatments, indicating that the ZrB₂ films were capable of withstanding the thermal stresses produced using rapid cooling from high temperatures during the experiments. In addition, the surface roughness was analyzed by AFM. AFM topography presents some columnar-like grain growth. Moreover, the root-mean-square (RMS) surface roughness values were estimated from 1 × 1 μm² AFM tiny region scans, and the measurements indicate a smooth surface with an RMS surface roughness below 1 nm. The RMS surface roughness is 0.287 nm for the as-grown sample and 0.469, 0.305, and 0.293 nm for the samples annealed at 750, 810, and 870 °C, respectively. The surface profile of ZrB₂ is rather smooth, in agreement with the SEM observations.

Figure 3a shows the cross-sectional bright-field TEM image of ZrB₂/Si(100) annealed at 870 °C. The cross-sectional transmission electron microscopy (XTEM, Philips Tecnai 20, Philips, Amsterdam, The Netherlands) images show that the ZrB₂ film grown on the Si(100) substrate is highly *c*-axis orientated from the film/substrate interface all the way to the film/vacuum interface. A smooth surface structure is clearly observed in the ZrB₂ film. In addition, the thickness of the ZrB₂ film was observed to be about 430 nm. In addition, a native oxide SiO_x layer was observed at the interface between the ZrB₂ film and the Si substrate. Figure 3b shows the High-resolution cross-sectional transmission electron microscopy (HR-XTEM) image of the ZrB₂ film, wherein the ZrB₂ film columns appear to be shifted by half a unit cell, which constitute stacking mismatch boundaries. Some stacking faults are also observed. Additionally, Figure 3c shows the Fast Fourier Transform (FFT) pattern calculated from Figure 3b, which reveals the ZrB₂ film is characterized by the hexagonal structure. Individual diffraction spots can be identified as ZrB₂ reflections, indicating that ZrB₂ film exhibits a highly preferred orientation. In addition, Figure 3d shows the Fourier-filtered image of the framed region in Figure 3c, obtained by

selecting the $\pm(0001)\text{ZrB}_2$ spots in the SAD pattern. The $d_{(0001)}$ spacing of ZrB_2 was determined from Figure 3d to be approximately 0.354 nm, which is close to the bulk ZrB_2 value of 0.353 nm [19].

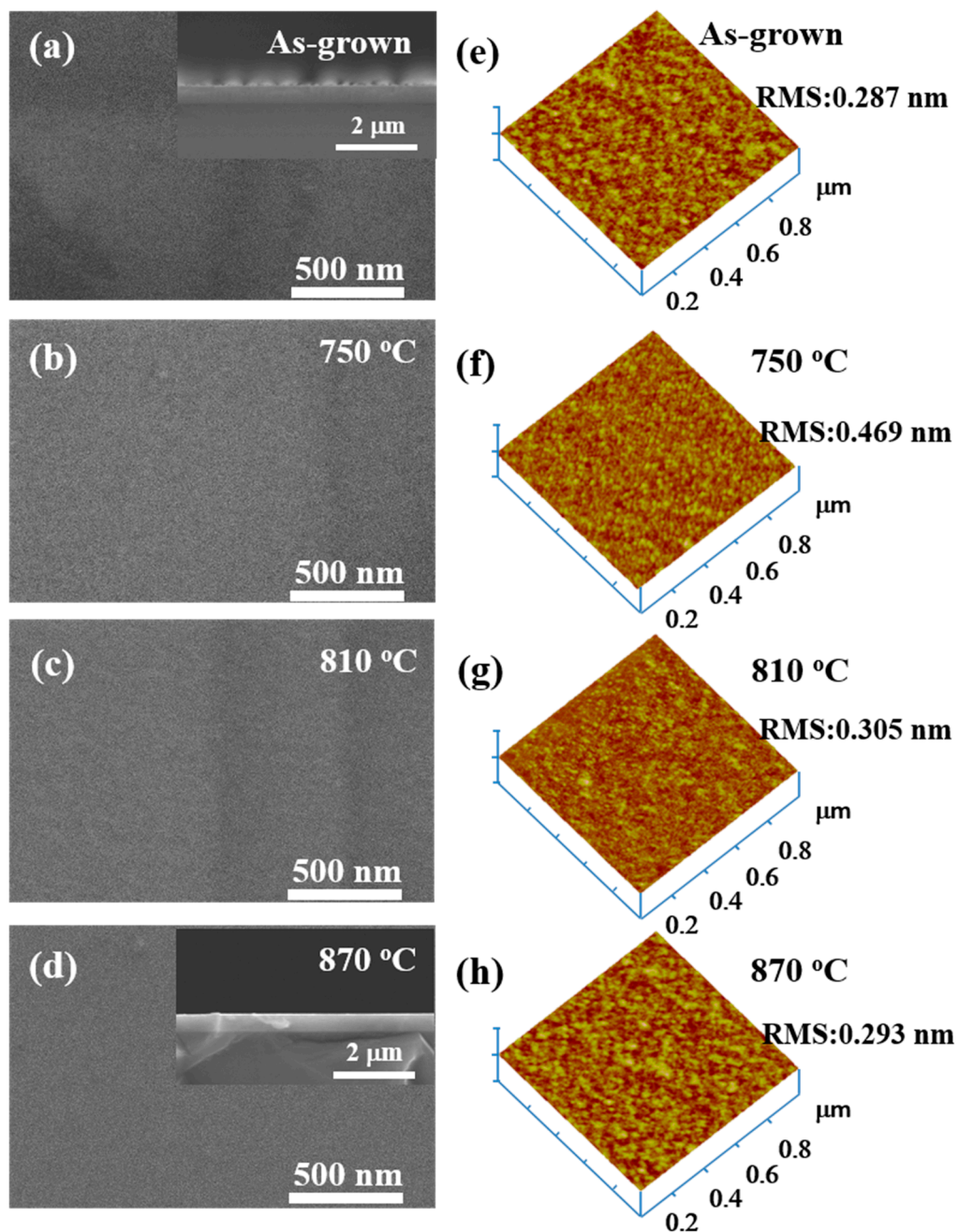


Figure 2. The cross-sectional and surface scanning electron microscopy (SEM) images (a–d) and atomic force microscopy (AFM) images of ZrB_2 films as grown and annealed at various temperatures (e–h): (a,e) as-grown, (b,f) 750 °C, (c,g) 810 °C and (d,h) 870 °C.

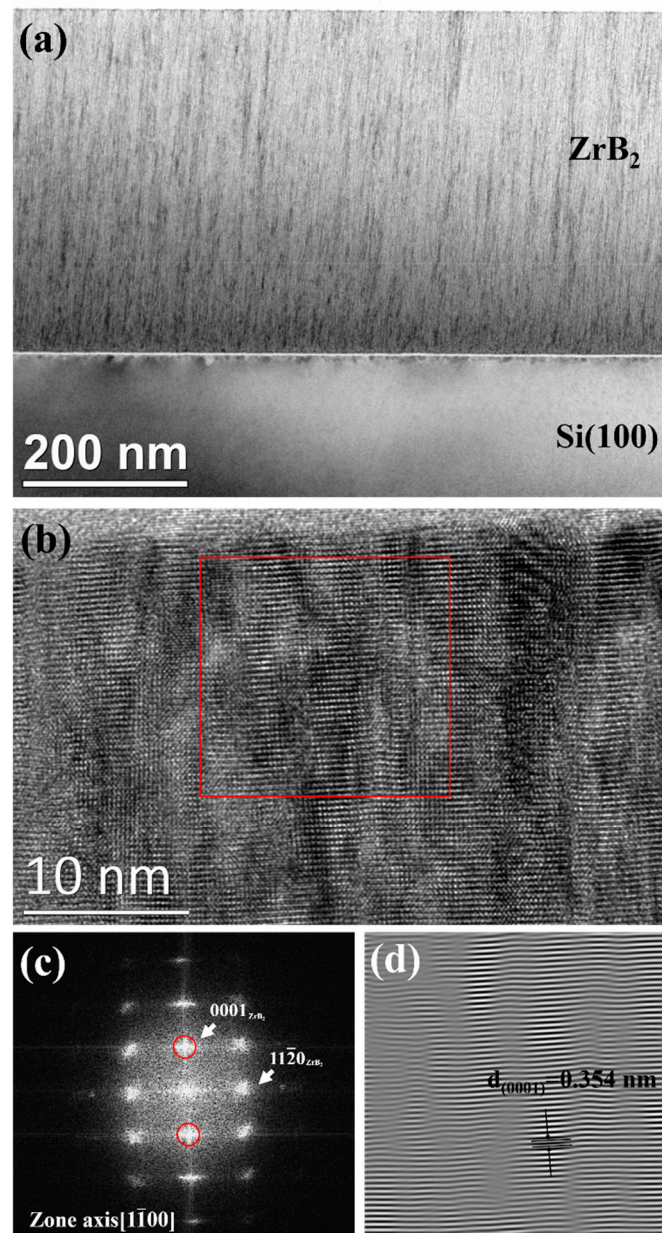


Figure 3. ZrB_2 film was annealed at 870 °C (a) The cross-sectional TEM image and (b) HR-XTEM image of ZrB_2 film. (c) the FFT pattern of the framed region in (b) red square. (d) Fourier-filtered image of the framed region in (c), obtained by selecting $\pm(0001)$ ZrB_2 and $\pm(11-20)$ ZrB_2 spots.

Figure 4 exhibits the TEM-Energy dispersive X-ray spectroscopy (EDS, Quantax, Bruker, Hamburg, Germany) line scan measured along the red line in the high-angle annular dark-field scanning transmission electron microscopy (HAADF-STEM, Tecnai G2 F20, FEI, Tokyo, Japan) image, which shows the ZrB_2 film and Si substrate. In the line scan results, the Zr profile shows a slightly higher concentration near the interface between the ZrB_2 film and the Si substrate. This result corresponds to the HAADF-STEM image. The average concentrations in the film regions are roughly estimated to be 55 ± 5 at % Zr and 25 ± 5 at % B. In addition, the EDS oxygen profiles display a slight peak in the oxygen concentration at the substrate–film interface (the red arrow in the inset of HAADF-STEM image). It is likely that a substantial part of this signal originates from sources other than the thin native oxide on the investigated Si(100) substrates, thus, indicating the presence of adsorbed oxygen-containing species on the substrate surfaces of the films deposited under these conditions.

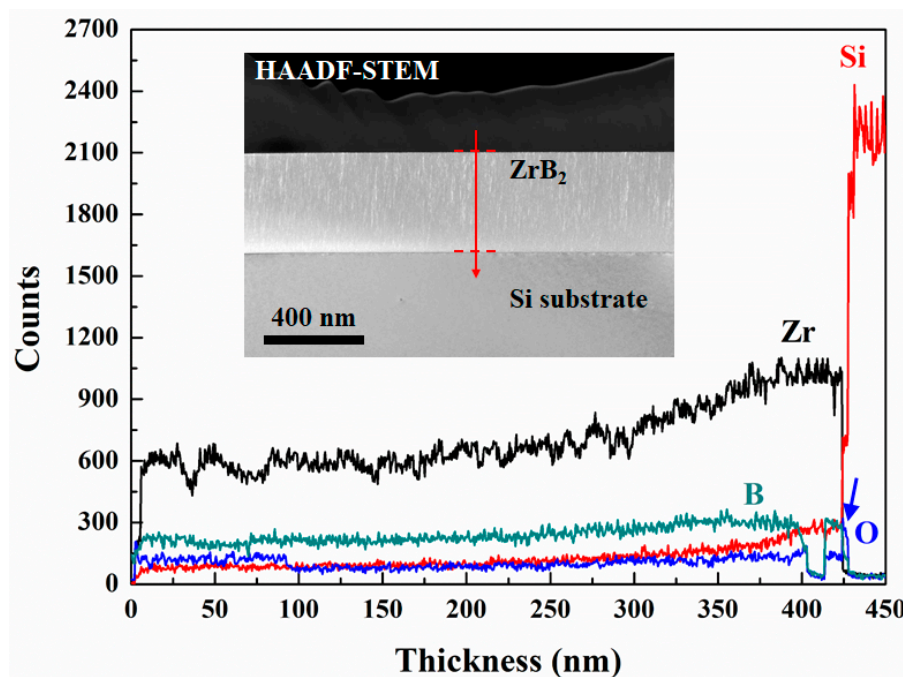


Figure 4. The TEM-EDS line scan measured along the depth of the ZrB_2 film. HAADF-STEM image shown in the inset of Figure 4. The inset shows that the ZrB_2 is uniformly distributed.

The chemical bonding structure and elemental composition of the ZrB_2 films were evaluated using XPS. Figure 5 shows the Zr 3d and B 1s regions of the XPS spectra of all the samples, which indicate the presence of ZrB_2 in the depth profile. The spin-orbit energy difference between the $3d_{5/2}$ and the $3d_{3/2}$ components is around 2.38 ± 0.02 eV. The binding energy of Zr $3d_{5/2}$ and Zr $3d_{3/2}$ located at 179.28, 181.68 ± 0.1 eV are attributed to the Zr–B bonds in a ZrB_2 compound [20]. The binding energy of Zr $3d_{5/2}$ and Zr $3d_{3/2}$ located at around 182.28 and 184.88 ± 0.1 eV are characteristic of the Zr–O bonds in oxide compounds [21,22]. Moreover, Zr–O was detected on the surface of films the as-grown film and those annealed at 750 and 810 °C. However, the Zr–O thin layer was undetected at the highest annealing temperature under vacuum. However, the Zr–O peak intensity decreases with the increasing annealing temperature. The estimated that of O atom adsorbed on the ZrB_2 surface forming a (2×2) super-structure but smaller than that of fully oxidized state Zr oxides [23]. The B1s peak appears at 187.9 eV, which agrees with the reported B1s energy in ZrB_2 [24]. These binding energies are in agreement with those determined for epitaxial ZrB_2 films deposited on 4H-SiC(0001) in Reference [25], with values of 179.0, 181.3, and 188.0 eV, respectively. Furthermore, the binding energies are consistent with values for single-crystal bulk ZrB_2 , i.e., 178.9, 181.3, and 187.9 eV, reported by Aizawa et al. [26] and 179.0, 181.4, and 188.0 eV reported by Singh et al. [27]. The XPS results suggest that the effective thickness of the native oxide layer on ZrB_2 decreased after annealing at 870 °C.

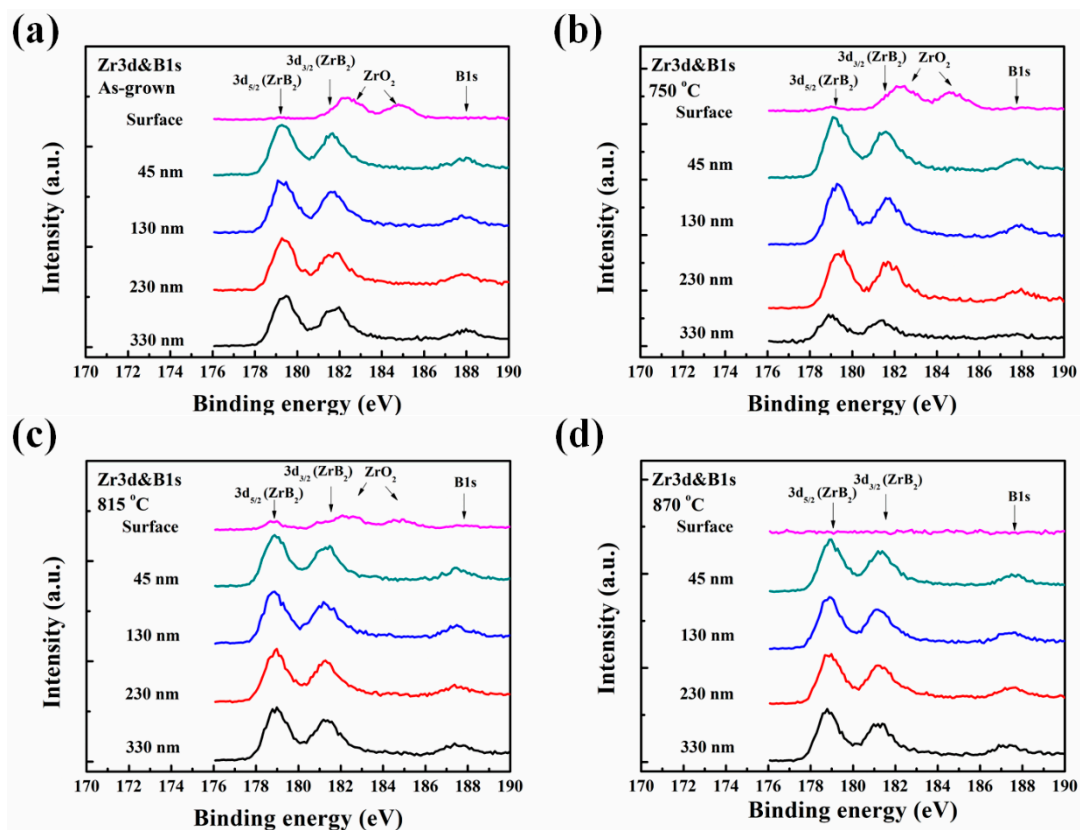


Figure 5. The Zr $3d$ and B $1s$ regions in the XPS spectra of the (a) as-grown ZrB_2 film and ZrB_2 films annealed at (b) $750\text{ }^\circ\text{C}$, (c) $815\text{ }^\circ\text{C}$, and (d) $870\text{ }^\circ\text{C}$.

4. Conclusions

Hexagonal ZrB_2 films can be deposited on mirror-like Si(100) substrate using pulsed DC magnetron sputtering. Additionally, sputtered ZrB_2 /Si films were annealed from 750 to $870\text{ }^\circ\text{C}$ in a vacuum chamber. Due to Zr-B bond not obviously changed, the annealing temperature on the chemical properties of the ZrB_2 film was found to be less affected for these results. The XRD patterns and TEM images indicated that the ZrB_2 films had good crystallinity and were highly oriented in the c -axis direction. In addition, the ZrB_2 crystallite size increased with the increasing annealing temperature. Additionally, the crystallite size of ZrB_2 slightly increased with the increasing annealing temperature. The SEM images and AFM measurements clearly demonstrated a smooth surface morphology on all ZrB_2 films. No morphological changes were observed after annealing the films and they retained their smoothness and homogeneity up to $870\text{ }^\circ\text{C}$. Finally, the surface morphologies of ZrB_2 films were exhibited with no obvious change with annealing temperatures in 750 – $870\text{ }^\circ\text{C}$. These findings indicate that vacuum annealing can slightly improve the structural properties of ZrB_2 films grown using DC magnetron sputtering. Therefore, the ZrB_2 film seems to be quite suitable as a buffer layer for III-nitride epitaxial growth.

Author Contributions: W.-C.C. carried out most of the experimental work including the ZrB_2 materials preparation, characterization, and drafted the manuscript. C.-T.L. helped the ZrB_2 growth. J.S. carried out the AFM measurements. H.-P.C. carried out the SEM measurements. All authors read and approved the manuscript.

Funding: This research was funded by the Ministry of Science and Technology, Taiwan under Contract Nos. 107-2111-E-492-001, MOST 107-2622-E-492-012-CC3.

Acknowledgments: The authors would like to thank T.Y. Yu carried out the high-resolution XPS measurements. S.Y. Kuo revised the manuscript.

Conflicts of Interest: The authors declare no conflict of interest.

References

1. Detchprohm, T.; Hiramatsu, K.; Itoh, K.; Akasaki, I. Relaxation process of the thermal strain in the GaN/ α -Al₂O₃ heterostructure and determination of the intrinsic lattice constants of GaN free from the strain. *Jpn. J. Appl. Phys.* **1992**, *31*, L1454–L1456. [[CrossRef](#)]
2. Wang, Z.T.; Yamada-Takamura, Y.; Fujikawa, Y.; Sakurai, T.; Xue, Q.K.; Tolle, J.; Kouvetakis, J.; Tsong, I.S.T. Effect of nitridation on the growth of GaN on ZrB₂(0001)/Si(111) by molecular-beam epitaxy. *J. Appl. Phys.* **2006**, *100*, 033506. [[CrossRef](#)]
3. Tomida, Y.; Nitta, S.; Kamiyama, S.; Amano, H.; Akasaki, I.; Otani, S.; Kinoshita, H.; Liu, R.; Bell, A.; Ponce, F.A. Growth of GaN on ZrB₂ substrate by metal-organic vapor phase epitaxy. *Appl. Surf. Sci.* **2003**, *216*, 502–507. [[CrossRef](#)]
4. Sun, Q.; Wang, J.; Wang, H.; Jin, R.; Jiang, D.; Zhu, J.; Zhao, D.; Yang, H.; Zhou, S.; Wu, M.; et al. High-temperature AlN interlayer for crack-free AlGaIn growth on GaN. *J. Appl. Phys.* **2008**, *104*, 043516. [[CrossRef](#)]
5. Sung, J.; Goedde, D.M.; Girolami, G.S.; Abelson, J.R. Remote-plasma chemical vapor deposition of conformal ZrB₂ films at low temperature: A promising diffusion barrier for ultralarge scale integrated electronics. *J. Appl. Phys.* **2002**, *91*, 3904–3911. [[CrossRef](#)]
6. Kamiyama, S.; Takanami, S.; Tomida, Y.; Iida, K.; Kawashima, T.; Fukui, S.; Iwaya, M.; Kinoshita, H.; Matsuda, T.; Yasuda, T.; et al. Violet and UV light-emitting diodes grown on ZrB₂ substrate. *Phys. Status Solidi A* **2003**, *200*, 67–70. [[CrossRef](#)]
7. Serban, E.A.; Palisaitis, J.; Junaid, M.; Tengdelius, L.; Högberg, H.; Hultman, L.; Persson, P.O.Å.; Birch, J.; Hsiao, C.L. Magnetron sputter epitaxy of high-quality GaN nanorods on functional and cost-effective templates/substrates. *Energies* **2017**, *10*, 1322. [[CrossRef](#)]
8. Tolle, J.; Roucka, R.; Tsong, I.S.T.; Ritter, C.; Crozier, P.A. Epitaxial growth of group III nitrides on silicon substrates via a reflective lattice-matched zirconium diboride buffer layer. *Appl. Phys. Lett.* **2003**, *82*, 2398–2400. [[CrossRef](#)]
9. Bera, S.; Sumiyoshi, Y.; Yamada-Takamura, Y. Growth of single-crystalline zirconium diboride thin film on sapphire. *J. Appl. Phys.* **2009**, *106*, 063531. [[CrossRef](#)]
10. Otani, S.; Korsukova, M.M.; Mitsunashi, T. Preparation of HfB₂ and ZrB₂ single crystals by the floating-zone method. *J. Cryst. Growth* **1998**, *186*, 582–586. [[CrossRef](#)]
11. Stewart, D.M.; Frankel, D.J.; Lad, R.J. Growth, structure, and high temperature stability of zirconium diboride thin films. *J. Vac. Sci. Technol. A* **2015**, *33*, 031505. [[CrossRef](#)]
12. Tengdelius, L.; Samuelsson, M.; Jensen, J.; Lu, J.; Hultman, L.; Forsberg, U.; Janzén, E.; Högberg, H. Direct current magnetron sputtered ZrB₂ thin films on 4H-SiC(0001) and Si(100). *Thin Solid Films* **2014**, *550*, 285–290. [[CrossRef](#)]
13. Sulyaeva, V.; Shestakov, V.; Romyantsev, Y.M.; Kosinova, M. Synthesis of zirconium diboride films and ZrB₂/BC_xN_y heterostructures. *Inorg. Mater.* **2018**, *54*, 133–139. [[CrossRef](#)]
14. Armitage, R.; Suda, J.; Kimoto, T. Characterization of ZrB₂(0001) surface prepared by ex situ HF solution treatment toward applications as a substrate for GaN growth. *Surf. Sci.* **2006**, *600*, 1439–1449. [[CrossRef](#)]
15. Samuelsson, M.; Jensen, J.; Helmersson, U.; Hultman, L.; Högberg, H. ZrB₂ thin films grown by high power impulse magnetron sputtering from a compound target. *Thin Solid Films* **2012**, *526*, 163–167. [[CrossRef](#)]
16. Janssen, G.C.A.M. Stress and strain in polycrystalline thin films. *Thin Solid Films* **2007**, *515*, 6654–6664. [[CrossRef](#)]
17. Kinoshita, H.; Otani, S.; Kamiyama, S.; Amano, H.; Akasaki, I.; Suda, J.; Matsunami, H. Zirconium diboride (0001) as an electrically conductive lattice-matched substrate for gallium nitride. *Jpn. J. Appl. Phys.* **2011**, *40*, L1280–L1282. [[CrossRef](#)]
18. Patterson, A.L. The scherrer formula for X-ray particle size determination. *Phys. Rev.* **1939**, *56*, 978–982. [[CrossRef](#)]
19. Li, H.; Zhang, L.; Zeng, Q.; Wang, J.; Cheng, L.; Ren, H.; Guan, K. Crystal structure and elastic properties of ZrB compared with ZrB₂: A first-principles stud. *Comp. Mater. Sci.* **2010**, *49*, 814–819. [[CrossRef](#)]
20. Alfano, D.; Scatteia, L.; Monteverde, F.; Beche, E.; Balat-Pichelin, M. Microstructural characterization of ZrB₂-SiC based UHTC tested in the MESOX plasma facility. *J. Eur. Ceram. Soc.* **2010**, *30*, 2345. [[CrossRef](#)]
21. Crist, B.V. *XPS Handbooks: The Elements and Native Oxides*; XPS International: Mountain View, CA, USA, 1999.

22. Gao, D.; Zhang, Y.; Fu, J.; Xu, C.; Song, Y.; Shi, X. Oxidation of zirconium diboride–silicon carbide ceramics under an oxygen partial pressure of 200 Pa: Formation of zircon. *Corros. Sci.* **2010**, *52*, 3297–3303. [[CrossRef](#)]
23. Aizawa, T.; Hishita, S.; Otani, S. The 2×2 oxidized layer on $ZrB_2(0001)$. *Appl. Surf. Sci.* **2009**, *256*, 1120–1123. [[CrossRef](#)]
24. Magnuson, M.; Tengdelius, L.; Greczynski, G.; Hultman, L.; Högberg, H. Chemical bonding in epitaxial ZrB_2 studied by X-ray spectroscopy. *Thin Solid Films* **2018**, *649*, 89–96. [[CrossRef](#)]
25. Tengdelius, L.; Greczynski, G.; Chubarov, M.; Högberg, H. Stoichiometric, epitaxial ZrB_2 thin films with low oxygen-content deposited by magnetron sputtering from a compound target: Effects of deposition temperature and sputtering power. *J. Cryst. Growth* **2015**, *430*, 55–62. [[CrossRef](#)]
26. Aizawa, T.; Suehara, S.; Hishita, S.; Otani, S.; Arai, M. Surface core-level shift and electronic structure on transition-metal diboride (0001) surfaces. *Phys. Rev. B* **2005**, *71*, 165405. [[CrossRef](#)]
27. Singh, R.; Trenary, M.; Paderno, Y. Analysis of a zirconium diboride single crystal, $ZrB_2(0001)$, by XPS. *Surf. Sci. Spectra* **2000**, *7*, 310–315. [[CrossRef](#)]



© 2019 by the authors. Licensee MDPI, Basel, Switzerland. This article is an open access article distributed under the terms and conditions of the Creative Commons Attribution (CC BY) license (<http://creativecommons.org/licenses/by/4.0/>).